On the Formation of Vinylamine ($C_2H_3NH_2$) in Interstellar Ice Analogs

Chaojiang Zhang[1,2], Jia Wang[1,2] , Andrew M. Turner[1,2], Joshua H. Marks[1,2], Sankhabrata Chandra[1,2],
Ryan C. Fortenberry[3] , and Ralf I. Kaiser[1,2]

[1] W. M. Keck Research Laboratory in Astrochemistry, University of Hawaii at Manoa, Honolulu, HI 96822, USA; ralfk@hawaii.edu
[2] Department of Chemistry, University of Hawaii at Manoa, Honolulu, HI 96822, USA
[3] Department of Chemistry & Biochemistry, University of Mississippi, University, MS 38677, USA; r410@olemiss.edu

Abstract

Amines—organic molecules carrying the –NH$_2$ moiety—have been recognized as a vital intermediate in the formation of prebiotic molecules such as amino acids and nucleobases. Here we report the formation of vinylamine ($C_2H_3NH_2$), which was recently detected toward G+0.693–0.027, in interstellar ice analogs composed of acetylene (C_2H_2) and ammonia (NH_3) exposed to energetic electrons. Our experiments mimic cascades of secondary electrons in the tracks of galactic cosmic rays impinging on interstellar ice in molecular clouds. Tunable photoionization reflectron time-of-flight mass spectrometry (PI-Re-TOF–MS), along with isomer-specific assignments, reveals the production of vinylamine ($C_2H_3NH_2$). Quantum chemical computations suggest that both a radical–radical recombination of the amino (NH_2) with the vinyl (C_2H_3) radical and a one-step concerted route are feasible pathways to vinylamine ($C_2H_3NH_2$). The results present the first documented route to form vinylamine in interstellar ice analogs. This unsaturated amine, which is isovalent to vinylalcohol (C_2H_3OH), could be a key precursor for the abiotic synthesis of prebiotic molecules such as amino acids and nucleobases, with implications for the origins-of-life theme.

1. Introduction

Ever since the first discovery of the cyano radical (CN) in the interstellar medium (ISM) more than 80 yr ago (McKellar 1940; Jefferts et al. 1970), nitrogen-bearing molecules such as primary amines—organic molecules carrying the amino (–NH$_2$) moiety—have attracted considerable attention from the astrochemistry, astrobiology, and planetary science communities (Zeng et al. 2018, 2021; Kolesniková et al. 2022; Rivilla et al. 2022; Sharma et al. 2023). This is due to their role as molecular building blocks of prebiotic molecules such as amino acids, nucleosides, and nucleotides, which are connected to the origins-of-life theme. As of now, only 10 molecules carrying the amino (–NH$_2$) moiety have been discovered or tentatively detected in extraterrestrial environments (Figure 1). These can be categorized as amines (R–NH$_2$), with R being a hydrocarbon group, and amides (R–CO–NH$_2$). Fully saturated amines, e.g., methylamine (CH$_3$NH$_2$; Fourikis et al. 1974; Bøgelund et al. 2019; Ohishi et al. 2019) and tentatively ethylamine (C$_2$H$_5$NH$_2$; Zeng et al. 2021), were observed toward the star-forming region SgrB2 and G+0.693–0.027, respectively. The recent detection of the unsaturated vinylamine (C$_2$H$_3$NH$_2$) toward G+0.693–0.027 represents a significant step toward advancing our understanding of prebiotic chemistry since the C=C–N backbone represents a fundamental building block of imidazole, which itself is a precursor to the nucleobase adenine (Zeng et al. 2021). The structural isomer ethanimine (CH$_3$CHNH) was itself observed toward the star-forming region SgrB2(N) (Loomis et al. 2013). Functionalized amines, in which a hydrogen atom of the hydrocarbon side chain is replaced by a functional group, have

also been detected. These are cyanamide (NH$_2$CN), aminoacetonitrile (NH$_2$CH$_2$CN), and more recently ethanolamine (NH$_2$CH$_2$CH$_2$OH) (Turner et al. 1975; Belloche et al. 2008; Rivilla et al. 2021). Besides amines, the amino group is also prominent in interstellar molecules carrying the peptide moiety including formamide (HCONH$_2$), acetamide (CH$_3$CONH$_2$), and urea ((NH$_2$)$_2$CO) toward SgrB2(N) (Rubin et al. 1971; Hollis et al. 2006; Kaiser et al. 2013; Frigge et al. 2018). Furthermore, recent laboratory studies propose the existence of aminomethanol (NH$_2$CH$_2$OH) and methanediamine (CH$_2$(NH$_2$)$_2$)—precursors to amino acids and nucleobases—in star-forming regions (Marks et al. 2022; Singh et al. 2022). In addition, liquid chromatography with fluorescence detection and time-of-flight mass spectrometry (LC-FD/TOFMS) on asteroid (162173) Ryugu return samples suggest the astrophysical presence of four aliphatic amines: methylamine (CH$_3$NH$_2$), ethylamine (C$_2$H$_5$NH$_2$), isopropylamine ((CH$_3$)$_2$CHNH$_2$), and propylamine (C$_3$H$_7$NH$_2$) (Naraoka et al. 2023; Parker et al. 2023).

However, despite the detection of vinylamine (C$_2$H$_3$NH$_2$) extending the possibilities to build nucleosides and nucleotides in extraterrestrial environments, its underlying formation routes are largely unknown. Gas-phase vinylamine (C$_2$H$_3$NH$_2$) was suggested to be produced via the reaction of the methylidyne radical (CH) with methylamine (CH$_3$NH$_2$; Zeng et al. 2018), but this reaction has not been explored in the laboratory. Furthermore, extensive networks of unstudied ion–molecule reactions including ethylamine (C$_2$H$_5$NH$_2$) were proposed (Zeng et al. 2021). However, extensive laboratory studies (Hagen et al. 1979; Moore & Donn 1982; Bernstein et al. 1995; Herbst 2014; Arumainayagam et al. 2019; Turner & Kaiser 2020) indicate that the majority of complex organic molecules (COMs) in star-forming regions are initially synthesized through the exposure of ice-coated interstellar grains composed of water (H$_2$O), methane (CH$_4$), methanol
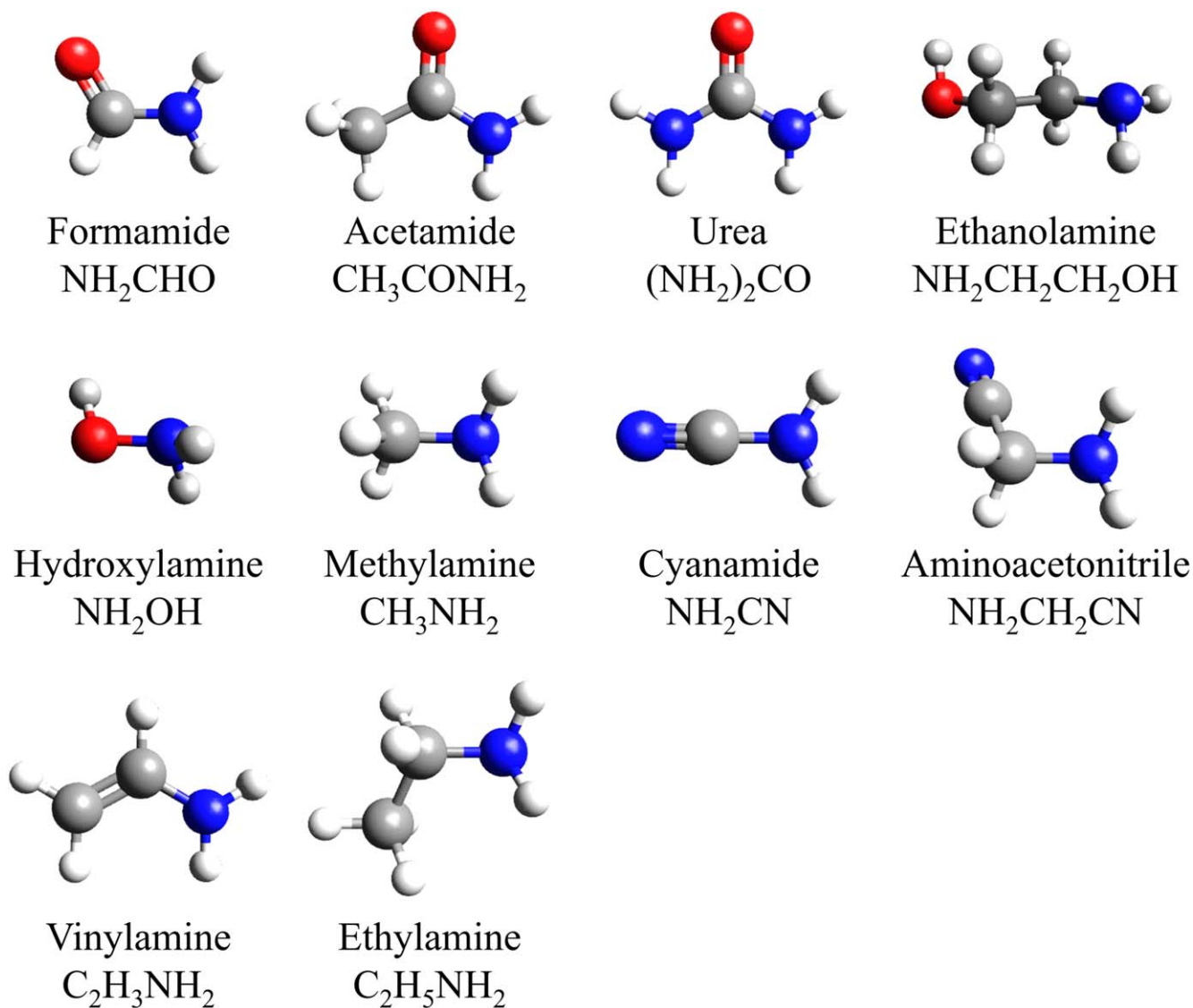
Figure 1. COMs carrying the amino (NH_2) moiety in extraterrestrial environments.

(CH_3OH), carbon monoxide (CO), carbon dioxide (CO_2), and ammonia (NH_3) (Boogert et al. 2015; Naden Robinson et al. 2017) to ionizing radiation, e.g., photons and galactic cosmic rays (GCRs) in molecular clouds. Several species, including carbon, oxygen, nitrogen, and sulfur elements, for example, glycolaldehyde enol, pyruvic acid, glycolic acid, and thioformic acid, have been produced in the interstellar ice analogs through nonequilibrium processes and detected in the gas phase (Morton & Kaiser 2003; Kleimeier et al. 2020, 2021a, 2021b; Wang et al. 2022; Marks et al. 2023), which provides a better understanding of the intrinsic formation pathways of COMs in molecular clouds. With respect to vinylamine ($C_2H_3NH_2$), however, no laboratory simulation experiment was successful in elucidating its underlying formation pathways.

The present work reveals the formation of vinylamine ($C_2H_3NH_2$) by exposing interstellar ice analogs composed of acetylene (C_2H_2) and ammonia (NH_3) mixtures to energetic electrons at a low temperature (10 K). The ice mixtures irradiated by energetic electrons mimic the processing by secondary electrons released during the passage of GCRs through interstellar ices (Forstel et al. 2015; Abplanalp & Kaiser 2020). Considering that only the saturated amines were

detected in the irradiated methane–ammonia system (Kim & Kaiser 2011; Förstel et al. 2017), here we chose the acetylene–ammonia ice mixture as reactants to produce the unsaturated vinylamine. Acetylene represents a major product in the radiolysis of methane (CH_4) ices (Kaiser & Roessler 1998; Bennett et al. 2006; Jones & Kaiser 2013; Abplanalp et al. 2018). Ammonia is the dominant nitrogen-bearing molecule in interstellar ices with abundances of up to 10% that of water (Boogert et al. 2015; McClure et al. 2023). The chemical modifications of the ice mixtures during the radiation exposure were traced in situ via Fourier transform infrared spectroscopy (FTIR; Nicolet 6700). The irradiated ice mixtures were then heated to 320 K to release molecules into the gas phase (temperature-programmed desorption (TPD)), where they were ionized isomer-selectively via vacuum ultraviolet (VUV) single photon ionization and mass resolved using a reflectron time-of-flight mass spectrometer (PI–Re–TOF–MS; Jones & Kaiser 2013; Abplanalp et al. 2015; Bergantini et al. 2018; Turner & Kaiser 2020). Isotopic substitution experiments and tunable photon ionization were exploited to probe the chemical formula and nature of the structural isomer formed.

2. Methods

2.1. Experimental Methods

The experiments were performed in an ultrahigh vacuum (UHV) chamber at pressures of a few 10^{-11} torr exploiting magnetically suspended turbo molecular pumps coupled with oil-free scroll backing pumps (Abplanalp et al. 2016; Turner & Kaiser 2020). A polished silver substrate was interfaced to a two-stage closed-cycle helium cryostat (Sumitomo Heavy Industries, RDK-415E) that can be freely rotated and translated vertically. After cooling the substrate to 10.0 ± 0.1 K, acetylene (C_2H_2, 99.9%, Airgas) and ammonia (NH_3, 99.999%, Matheson) were introduced into the main chamber via a pair of glass capillary arrays at a pressure of 2×10^{-8} torr and deposited onto the surface of low-temperature wafer. Laser interferometry was used to determine the total ice thickness with a helium–neon (HeNe) laser operated at 632.8 nm with a 4° angle of incidence and measuring variations in reflected power due to thin film interference during the ice deposition (Turner et al. 2015). Considering the refractive index of 1.34 ± 0.01 for acetylene at 12 K and of 1.38 ± 0.03 for ammonia at 13 K (Satorre et al. 2013; Hudson et al. 2014), the refractive index of the acetylene–ammonia ice mixture can be approximated to 1.36 ± 0.02 by a weighted average of those values of the two components. The thickness of the deposited acetylene–ammonia ice was derived to be 1000 ± 100 nm. FTIR spectra (Thermo Electron, Nicolet 6700) were measured in the range of 6000–500 cm^{-1} after ice mixture deposition to calculate the ratio of the acetylene and ammonia components. The FTIR spectrometer was operated in absorption-reflection-absorption mode at a reflection angle of 45° using a resolution of 4 cm^{-1} with 220 scans per spectrum. The ice ratio of acetylene to ammonia was determined to be $1:1 \pm 0.2$ by accounting for the integrated absorption coefficients of the ν_5 mode at 758 cm^{-1} (2.4×10^{-17} cm molecule^{-1}) and the ν_3 mode at 3239 cm^{-1} (2.4×10^{-17} cm molecule^{-1}) for acetylene (Hudson et al. 2014), along with the ν_2 mode at 1071 cm^{-1} (2.1×10^{-17} cm molecule^{-1}), ν_4 mode at 1626 cm^{-1} (5.6×10^{-18} cm molecule^{-1}), and ν_3 mode at 3394 cm^{-1} (2.3×10^{-17} cm molecule^{-1}) for ammonia (Bouilloud et al. 2015). It is necessary to mention that these absorption coefficients are obtained from IR transmission spectra and we use them in reflection as a means to estimate the ratio of components in our ice mixture. The ice mixtures were then irradiated at 10.0 ± 0.1 K by 5 keV electrons scanned over an area of 1.0 ± 0.1 cm^2 at an angle of incidence of 70° relative to the surface normal at a current of 10 nA for 5 minutes. The average penetration depth of the energetic electrons was simulated via Monte Carlo simulations (CASINO; Drouin et al. 2007) to be 350 ± 30 nm. Since this penetration depth is less than the thickness of the deposited ice (1000 ± 100 nm), the energetic electrons only interact with the ice, but not with the silver substrate. The average dose is calculated to be 0.040 ± 0.007 eV per acetylene molecule and 0.030 ± 0.005 eV per ammonia molecule (Table 1), thus simulating the exposure of interstellar ices of $(3.8 \pm 0.5) \times 10^4$ yr in cold molecular clouds (Holtom et al. 2005). During the electronic irradiation, the functional groups of compounds in the ice mixtures were monitored by the FTIR spectra.

After the electron irradiation, TPD was performed to sublime the ice mixtures along with the newly formed products. Each irradiated sample was heated to 320 K at a rate of 1 K minute^{-1}.

Table 1
Parameters Used in Dosage Calculation and Resulting Doses

| Parameter		Value
Initial Kinetic Energy of the Electrons, E_{init} (keV)		5
Ice mixtures		acetylene–ammonia
Ice mixtures ratios		$1:1 \pm 0.2$
Density of ice (gm cm^{-3})		0.74 ± 0.02
Thickness of ice (nm)		1000 ± 100
Average penetration depth, l_{ave} (nm)[a]		350 ± 30
Maximum penetration depth, l_{max} (nm)		700 ± 50
Average kinetic energy of backscattered electrons, E_{bs} (keV)[a]		1.1 ± 0.2
Average kinetic energy of transmitted electrons, E_{trans} (keV)[a]		0
Irradiated area, A (cm^2)		1.0 ± 0.1
Irradiation current, I (nA)		10
Irradiation time, t (s)		300
Dose (eV molecule^{-1})	Acetylene	0.04 ± 0.007
	Ammonia	0.03 ± 0.005

Note.
[a] Parameters obtained using the CASINO software v2.42.

During the TPD phase, a reflectron time-of-flight mass spectrometer (Re-TOF–MS, Jordan TOF Products, Inc.) coupled with photoionization (PI) at photon energies of 9.80, 9.34, 9.18, 8.50, and 7.90 eV was utilized to ionize the subliming molecules. These photon energies were chosen based on the ionization energies (IEs) for isomers of vinylamine (Tables A1 and A2). To generate these photons, a pulsed (30 Hz) coherent VUV light was achieved via four-wave mixing using Krypton (Specialty Gases, 99.999%) or Xenon (Specialty Gases, 99.999%) as a nonlinear medium (Table 2). The VUV light was separated using a lithium fluoride (LiF) biconvex lens (ISP Optics) based on distinct refractive indices of the lens material for different wavelengths (VonDrasek et al. 1988). The photoionized molecules were extracted, and mass-to-charge ratios (m/z) were determined based on the arrival time of the ions at a multichannel plate. The signal was amplified with a fast preamplifier (Ortec 9305) and recorded using a bin width of 4 ns that was triggered at 30 Hz (Quantum Composers, 9518). FTIR and PI–Re-TOF–MS assignments were cross-checked and verified with ices containing isotopically substituted counterparts: $^{15}NH_3$ ($^{15}NH_3$, >98 ^{15}N%, Sigma Aldrich) and C_2D_2 (C_2D_2; >99 D%, C/D/N Isotope).

2.2. Computational Methods

The quantum chemical computations rely on the CCSD(T) method (Raghavachari et al. 1989) and the aug-cc-pVTZ basis set (Kendall et al. 1992; Peterson & Dunning 1995) in large part. The geometries are optimized, and subsequent harmonic frequencies are computed at the CCSD(T)/aug-cc-pVTZ level. The energies are calculated by employing two-point complete basis set (CBS) limit extrapolations (Martin & Lee 1996) for the optimized CCSD(T)/aug-cc-pVTZ energy and a single-point CCSD(T)/aug-cc-pVQZ energy at the optimized CCSD (T)/aug-cc-pVTZ geometry and corrected for zero-point vibrational energy (ZPVE) obtained from the optimized CCSD(T)/aug-cc-pVTZ geometry. The transition states (TSs) are optimized and harmonic analysis undertaken with B3LYP/aug-cc-pVTZ (Becke 1988; Lee et al. 1988; Becke 1993) in order to make sure that there is only one imaginary frequency.
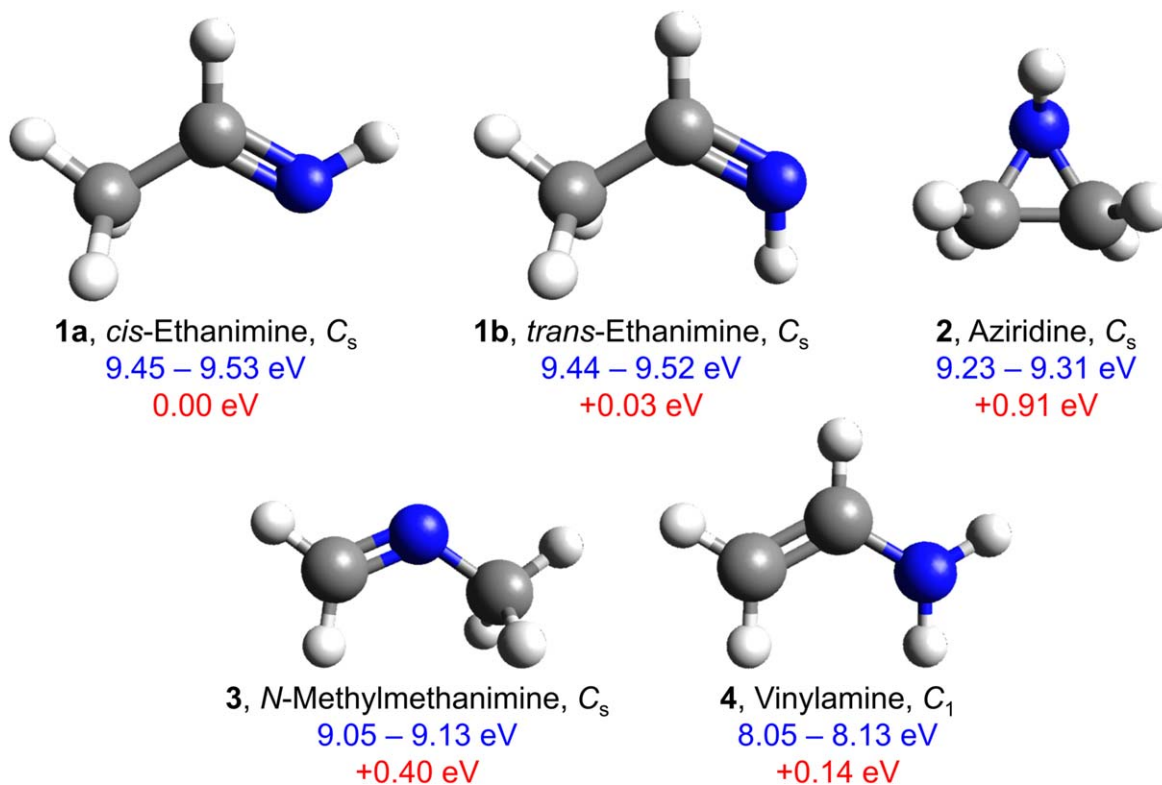
Figure 2. Geometries of C_2H_5N isomers optimized at the B3LYP/aug-cc-pVTZ level of theory. The adiabatic IEs (blue values) are computed at the CCSD(T)/CBS level of theory with correction by ZPVE corrections obtained at the B3LYP/aug-cc-pVTZ level; computed IEs are corrected by incorporating the error analysis (Tables A1 and A2). Relative energies (red values) at the CCSD(T)/CBS level and point groups of each isomer are also shown.

Table 2
Parameters for the Generation of Vacuum Ultraviolet Light

VUV	Photoionization Energy (eV)	9.80 ($2\omega_1 - \omega_2$)	9.34 ($2\omega_1 - \omega_2$)	9.18 ($2\omega_1 - \omega_2$)	8.50 ($2\omega_1 - \omega_2$)	7.90 ($2\omega_1 - \omega_2$)
	Wavelength (nm)	114.588	132.745	135.059	145.864	156.942
ω_1	Wavelength (nm)	202.316	111.283	111.283	202.316	202.316
Nd:YAG	Wavelength (nm)	532	355	355	532	532
Dye laser	Wavelength (nm)	606.948	445.132	445.132	606.948	606.948
Dye1		R610/R640/EtOH	C450/EtOH	C450/EtOH	R610/R640/EtOH	R610/R640/EtOH
ω_2	Wavelength (nm)	504.725	688.305	632.154	330.055	284.598
Nd:YAG	Wavelength (nm)	355	532	532	532	532
Dye laser	Wavelength (nm)	504.725	688.305	632.154	660.110	569.196
Dye2		C503/EtOH	LDS698/EtOH	DCM/EtOH	DCM/DMSO	P580/EtOH
	Nonlinear medium	Krypton	Xeon	Xeon	Krypton	Krypton

**Note.** The uncertainty for VUV photon energies is less than 0.005 eV.

Energies on the reported reaction pathway are relative to the acetylene and ammonia reactants. The calculations of the CCSD(T)/CBS method are conducted via the MOLPRO2020 program (Werner et al. 2012, 2020), and the B3LYP/aug-cc-pVTZ computations originate from the *Gaussian16* code (Frisch et al. 2016).

3. Results

3.1. Geometries of C_2H_5N Isomers

Quantum chemistry calculations indicated four structural isomers of the molecular formula of C_2H_5N (Figure 2). Recall that ethanimine (1a/1b) and vinylamine (4) have been identified in the ISM (Loomis et al. 2013; Zeng et al. 2021). The CCSD(T)/CBS computations reveal that ethanimine (1) represents the global minimum with an energy difference between *cis/trans*-ethanimine close to 3 kJ mol^{-1} (0.03 eV). Vinylamine (4) is less stable by 14 kJ mol^{-1} (0.14 eV), while the relative energies of aziridine (2) and *N*-methylmethanimine (3) were computed to be 88 kJ mol^{-1} (0.91 eV) and 39 kJ mol^{-1} (0.40 eV). Previous calculations at the MP2/6–311G++(d, p) level (Sil et al. 2018) suggested a similar trend with *cis*-ethanimine (1a) lower than *trans*-ethanimine (1b) by 4 kJ mol^{-1}. Quan et al. (2016) and Loomis et al. (2013) obtained energy differences between conformers *cis*-ethanimine (1a) and *trans*-ethanimine (1b) of 5 and 4 kJ mol^{-1} at the B3LYP/aug-cc-pVTZ and MP2/6–311G++(d, p) level of theory, respectively, implying that the current results are reliable and should be the most accurate produced to date.
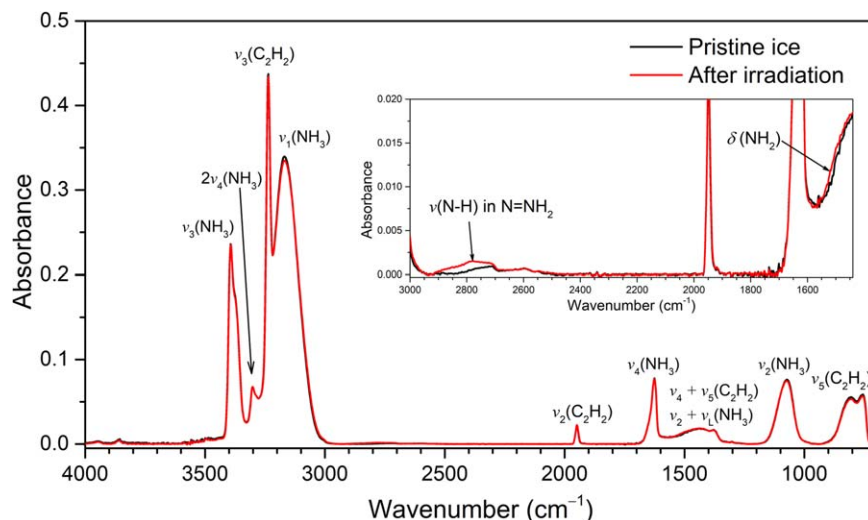
Figure 3. The infrared spectra of acetylene–ammonia ice mixtures before (black) and after (red) irradiation. Detailed assignments were compiled in Table 3.

3.2. FTIR

Figure 3 displays the FTIR spectra of the acetylene–ammonia ice mixtures before (black) and after (red) irradiation at 10 K and the absorptions features are compiled in Table 3. To confirm weak new absorption features, we plot the difference spectrum of the acetylene−ammonia ice mixture before and after irradiation in Figure A1. The FTIR spectra for isotopically labeled ices (C_2D_2–NH_3, C_2H_2–$^{15}NH_3$) before and after irradiation are shown in Figure A2 along with newly obtained peaks (Table A3). Overall, both spectra are dominated by the fundamentals of acetylene (ν_5, 758 cm^{-1}; ν_2, 1948 cm^{-1}; ν_3, 3239 cm^{-1}) and ammonia (ν_2, 1071 cm^{-1}; ν_4, 1626 cm^{-1}; ν_1, 3187 cm^{-1}; ν_3, 3394 cm^{-1}) along with their combination modes and overtones for acetylene ($\nu_4 + \nu_5$, 1306 cm^{-1}; $\nu_2 + \nu_5$, 2752 cm^{-1}) and ammonia ($2\nu_4$, 3303 cm^{-1}). A band at 1466 cm^{-1} assigned to combination modes, including lattice mode ($\nu_2 + \nu_L$), was also observed. After irradiation, a couple of new weak peaks emerged. The new peak at 2791 cm^{-1} can be linked to the N–H stretching mode in N=NH_2, and the new signal at 1512 cm^{-1} observed from the difference infrared spectrum (Figure A1) is connected to the –NH_2 scissor mode (Zheng et al. 2008; Kim & Kaiser 2011). Apart from the –NH_2 scissor mode, which is not allowed to identify any individual molecules, no evidence of vinylamine was found in the FTIR spectra of the irradiated acetylene–ammonia ice mixture. These infrared data provide information on the *functional groups* of newly formed molecules, but in the case of complex ice mixtures, FTIR cannot assign individual molecules (Abplanalp et al. 2016; Zhu et al. 2018). Therefore, in order to identify individual molecules formed in these complex ice mixtures, an alternative analytical approach is required to isomer-selectively assign newly prepared molecules.

3.3. PI−Re-ToF−MS

Photoionization reflectron time-of-flight mass spectrometry (PI-Re-ToF–MS) was exploited during the TPD phase to unravel the nature of the structural isomer(s) formed. Compared to FTIR, this approach can discriminate structural isomers based on distinct adiabatic IEs of the C_2H_5N isomers ($m/z = 43$, Figure 2) by systemically tuning the photon energies *above* and *below* the isomer of interest (Abplanalp et al. 2016; Zhu et al. 2018). Considering the
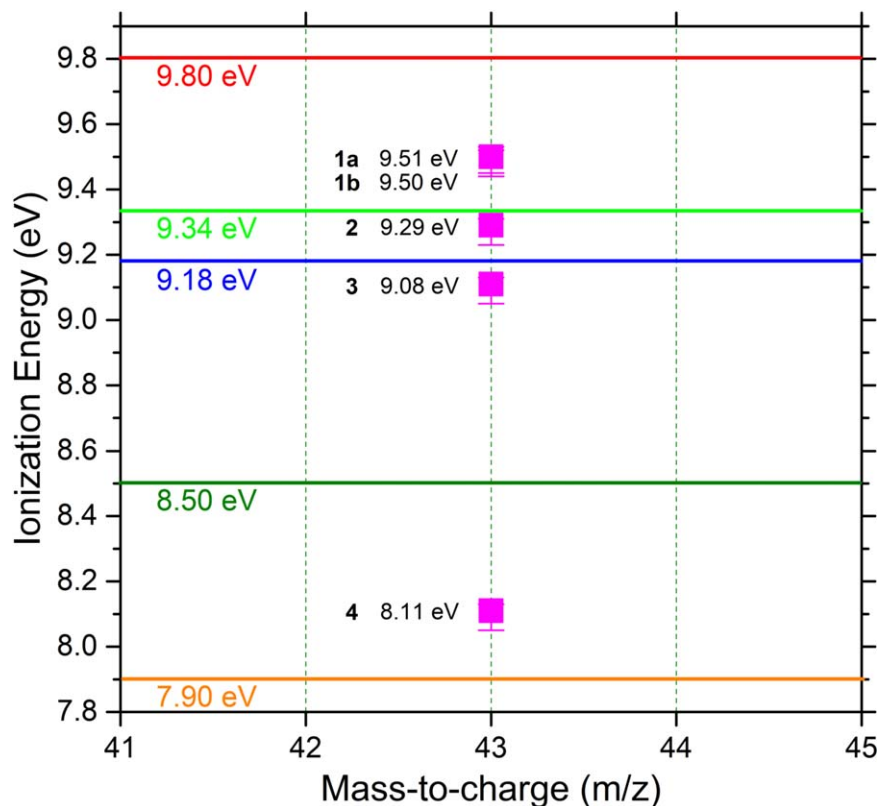
Table 3
Infrared Absorption Features Were Recorded before and after the Irradiation of Acetylene–Ammonia Ice Mixtures at 10 K

Absorption Peaks (cm^{-1})	New Absorption Peaks after Irradiation (cm^{-1})	Assignment	Reference
758		C_2H_2 (ν_5)	1
1071		NH_3 (ν_2)	2
1304, 1466		C_2H_2 ($\nu_4+\nu_5$) NH_3 ($\nu_2+\nu_L$)	1
	1512	δ (NH_2)	2, 3
1626		NH_3 (ν_4)	2
1948		C_2H_2 (ν_2) C_2H_2 ($2\nu_4+\nu_5$)	1
2752		C_2H_2 ($\nu_2+\nu_5$)	1
	2791	N–H stretching in N=NH_2	2
3187		NH_3 (ν_1)	2
3239		C_2H_2 (ν_3)	1
3303		NH_3 ($2\nu_4$)	2
3394		NH_3 (ν_3)	2

References. (1) Abplanalp & Kaiser 2020; (2) Zheng et al. 2008; (3) Socrates 2004.

computed IEs of the C_2H_5N isomers, five photon energies of 9.80, 9.34, 9.18, 8.50, and 7.90 eV were employed (Figure 4). Photons at 9.80 eV can ionize *all* C_2H_5N isomers; 9.34 eV photons can ionize isomers 2, 3, and 4; and photons at 9.18 eV can photoionize only isomers 3 and 4. Finally, 8.50 eV photons can only ionize isomer 4, while 7.90 eV photons cannot ionize any isomers. The PI–Re-ToF–MS data are compiled in Figure 5. To determine the molecular formula for the signal at $m/z = 43$, two separate experiments replacing ammonia and acetylene with ^{15}N–ammonia ($^{15}NH_3$) and D_2–acetylene (C_2D_2) were also conducted (Figures 6(a) and (b)). The ^{15}N–ammonia ($^{15}NH_3$) reactant shifts the TPD profile from $m/z = 43$ to 44, whereas the D_2–acetylene reactant moves the ion counts from $m/z = 43$ to 45. These findings reveal that the carrier of the ions at $m/z = 43$ contains one nitrogen atom and two hydrogen atoms from acetylene. Therefore, the molecular formula of this species can be assigned to C_2H_5N. In the TPD profile

Figure 4. Calculated adiabatic IEs of C_2H_5N isomers along with error limits (Table A2). VUV photon energies at 9.80, 9.34, 9.18, 8.50, and 7.90 eV were exploited to distinguish different isomers of C_2H_5N.

recorded at $m/z = 44$ of the C_2H_2–$^{15}NH_3$ system, a shoulder at 146 K was observed. This peak can belong to photofragments from species at $m/z = 78$ ($C_2H_9^{15}N_3$, Figure 7(a)). Similarly, in the TPD profile recorded at $m/z = 45$ of the C_2D_2–NH_3 system, a shoulder at 151 K was observed, caused by photofragments from species at $m/z = 84$ ($C_4D_4N_2$, Figure 7(b)). The TPD profiles of C_2H_5N at $m/z = 43$ recorded at photon energies of 9.80, 9.34, 9.18, 8.50, and 7.90 eV were extracted and normalized (Figures 6(c) and (d)). All the TPD profiles at $m/z = 43$ show signals at 9.80, 9.34, 9.18, and 8.50 eV, revealing overlapping sublimation events peaking at 133 K (Figure 4(d)). No ion signal at $m/z = 43$ was detected at a photon energy of 7.90 eV. Therefore, the detected ions monitored at 9.80, 9.34, 9.18, and 8.50 eV can only be connected to vinylamine ($C_2H_3NH_2$, 4). These findings provide compelling evidence for the formation of vinylamine ($C_2H_3NH_2$) and detection in the acetylene–ammonia processed ices. Critically, control experiments were also conducted without exposing the ice mixtures to energetic electrons at 10 K followed by photoionization by photons of energy 10.49 eV during the TPD phase. In these control experiments, no ion counts were observed at $m/z = 43$ (Figure 6(c), blank 10.49 eV), revealing that the observed ion counts at $m/z = 43$ in other experiments are linked to the energetic processing of the ice mixtures but not the result of ion–molecule reactions during photoionization of the sublimated acetylene and ammonia gases. Note that this control experiment is used to state that vinylamine is a product of irradiation on the acetylene–ammonia ice mixture; in addition, thermal reactions do not happen in the ice during the TPD phase of the nonirradiated ice experiment.

4. Discussion

Having provided persuasive evidence on the formation of vinylamine ($C_2H_3NH_2$, 4) through exposing acetylene–ammonia ice mixtures to electronic irradiation, potential formation routes are now proposed by merging the experimental data with quantum chemical computations (Figure 8). Previous experiments in pure ammonia ice revealed that, upon interaction with energetic electrons, ammonia can decompose via atomic hydrogen loss to form the amino radical (Zheng et al. 2008) through reaction (1). This process is endoergic by 454 kJ mol^{-1} with the energy for the bond cleavage supplied by the impinging electrons:

$$NH_3 \rightarrow \dot{N}H_2 + H \tag{1}$$

$$HCCH + H \rightarrow C_2H_3 \tag{2}$$

$$H_2\dot{C}CH + \dot{N}H_2 \rightarrow CH_2CHNH_2. \tag{3}$$
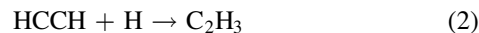
The suprathermal hydrogen atom can add to the carbon–carbon triple bond of acetylene, leading to the formation of the vinyl radical (C_2H_3) via reaction (2). The suprathermal nature of the hydrogen atom is critical to overcome the barrier to the addition of 18 kJ mol^{-1} (Kaiser & Roessler 1998; Miller & Klippenstein 2004). The amino radical and vinyl radical can then form vinylamine ($C_2H_3NH_2$) through a barrierless radical–radical recombination (Figure 8) via reaction (3) if they have a favorable geometry for recombination in the ice mixtures. Besides the radical pathway, the computations revealed a molecular addition pathway to vinylamine. Here the calculations expose a van der Waals complex (i3) stabilized by 11 kJ mol^{-1} with respect to the separated reactants (Figure 8). This complex can undergo a one-step, molecular addition producing vinylamine via a TS located 140 kJ mol^{-1}
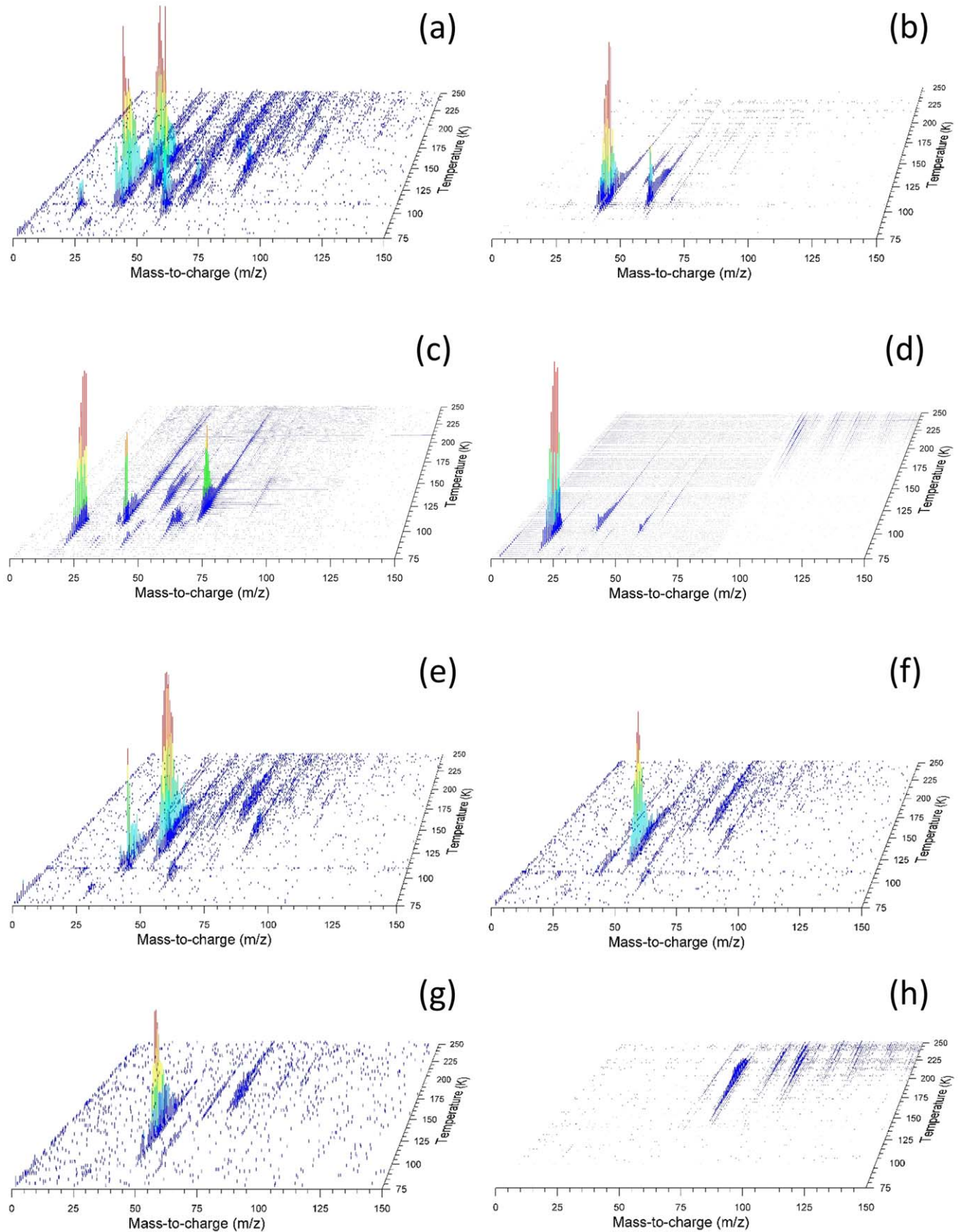
Figure 5. Photoionization reflectron time-of-flight mass spectra (PI–Re-TOF–MS) collected during the TPD phase of irradiated acetylene–ammonia ice mixtures. (a) C_2H_2–NH_3 experiment (photon energy 9.80 eV). (b) C_2H_2–$^{15}NH_3$ experiment (photon energy 9.80 eV). (c) C_2D_2–NH_3 experiment (photon energy 9.80 eV). (d) C_2H_2–NH_3 blank experiment (photon energy 10.49 eV). (e) C_2H_2–NH_3 experiment (photon energy 9.34 eV). (f) C_2H_2–NH_3 experiment (photon energy 9.18 eV). (g) C_2H_2–NH_3 experiment (photon energy 8.50 eV). (h) C_2H_2–NH_3 experiment (photon energy 7.90 eV).
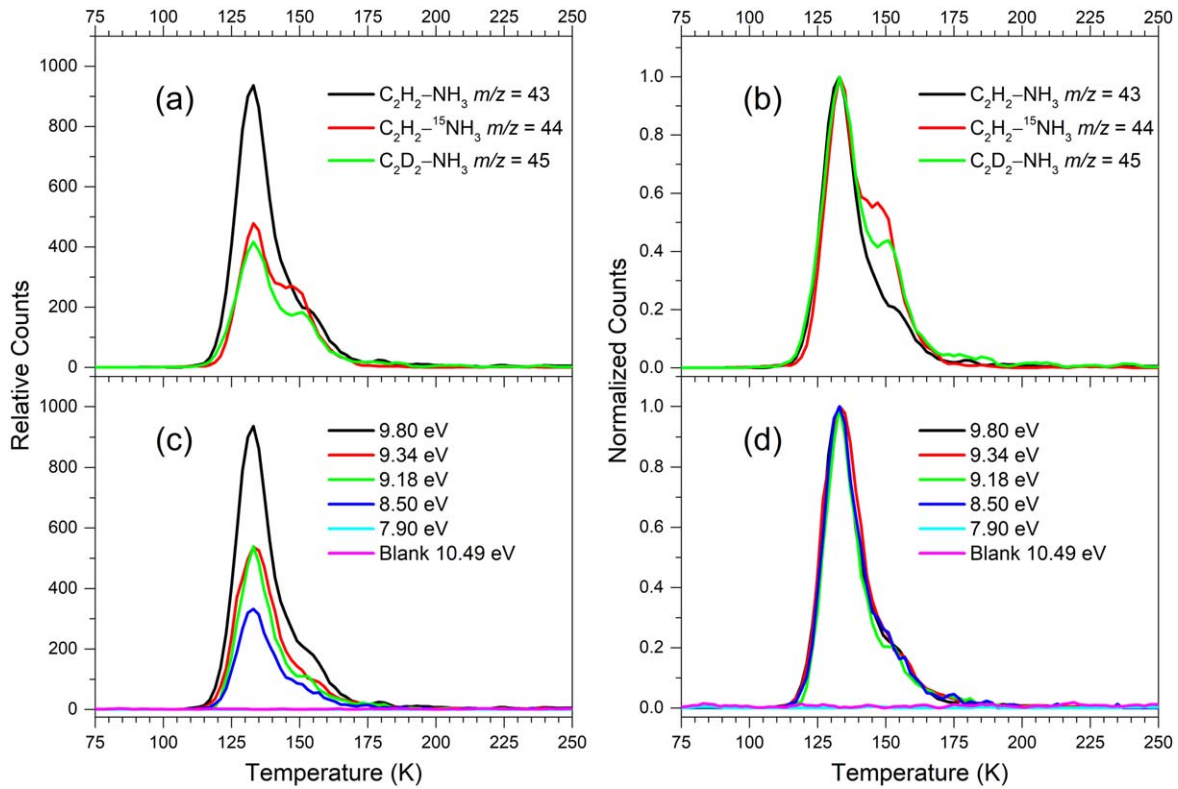
Figure 6. TPD profiles of vinylamine molecules. (a) TPD profiles for C_2H_5N, $C_2H_5^{15}N$, and $C_2D_2H_3N$ at a photon energy of 9.80 eV. (b) TPD profiles for C_2H_5N, $C_2H_5^{15}N$, and $C_2D_2H_3N$ at a photon energy of 9.80 eV with normalized counts. The shoulder peak of $C_2H_5^{15}N$ (red line in B) and $C_2D_2H_3N$ (green line in B) originates from the photofragmentation of $C_2H_9^{15}N_3$ and $C_4D_4N_2$, respectively (Figure 6). (c) TPD profiles for $m/z = 43$ (C_2H_5N) at different photon energies. (d) TPD profiles for $m/z = 43$ (C_2H_5N) at different photon energies with normalized counts.

above the van der Waals complex. Overall, the formation of vinylamine from acetylene–ammonia is exoergic by 121 kJ mol^{-1}.

5. Astrophysical Implications

This combined experimental and computational study demonstrates that vinylamine—a potential building block to nucleosides and nucleotides—can form in interstellar ice analogs containing acetylene and ammonia through exposure to proxies of GCRs in the form of energetic electrons equivalent to time spans of $(3.8 \pm 0.5) \times 10^4$ yr. In molecular clouds this would correspond to the early stage of an interstellar molecular cloud with a typical lifetime of up to 10^7 yr (Strazzulla & Johnson 1991; Yeghikyan 2011). Vinylamine was synthesized at 10 K first and then sublimed in the TPD phase, which mimics the transition from a cold molecular cloud to star-forming regions. Although acetylene has not been identified in interstellar ices, laboratory studies provide explicit evidence that acetylene represents a major reaction product of the radiolysis and photolysis of methane (CH$_4$) ice (Kaiser & Roessler 1998; Bennett et al. 2006; Jones & Kaiser 2013; Abplanalp et al. 2018), which has been detected in interstellar ice with abundance up to 11% relative to water (Boogert et al. 2015). Ammonia has also been observed in interstellar ice with abundances up to 10% relative to water (Boogert et al. 2015; McClure et al. 2023). Our study provides the first documented route to form vinylamine as detected at fractional abundances of $(3.3 \pm 0.4) \times 10^{-10}$ relative to molecular hydrogen toward G+0.693–0.027 (Zeng et al. 2021).

The nonequilibrium chemistry in the acetylene and ammonia ice mixtures reveals that vinylamine ($C_2H_3NH_2$) can form in the early stage of molecular clouds and then sublime into the gas phase during the transition to star-forming regions with detection enabled by radio telescopes (Zeng et al. 2021). Furthermore, vinylamine can be involved in the evolution of molecular precursors connected to the origins-of-life theme in deep space since it represents an important molecular building block of the nitrogen bases of deoxyribonucleic acid and ribonucleic acid (imidazole, adenine, thymine, guanine). Those simple prebiotic molecules may also sublime to be incorporated into planetoids, asteroids, and comets in the star-forming regions, which can be eventually delivered to early Earth through meteoritic parent bodies such as the Murchison meteorite, supporting the hypothesis of an exogenous origin and delivery of biologically important molecules to early Earth (Shimoyama & Ogasawara 2002). In addition, acetylene and ammonia molecules, along with acetylene–ammonia co-crystals, have been proposed in Titan's atmosphere and on Titan's surface by the Cassini-Huygens mission (Fulchignoni et al. 2005; Waite et al. 2005; Coustenis et al. 2007; Niemann et al. 2010; Yelle et al. 2010; Singh et al. 2016; Cable et al. 2018; Thakur & Remsing 2023). The formation of vinylamine through the exposure of acetylene and ammonia ice mixtures to GCR proxies suggests that vinylamine can form on the Titan's surface by GCR-triggering chemistry and may even be involved in a chain of complex chemical reactions leading eventually to biomolecules, for example, amino acids and nucleobases.
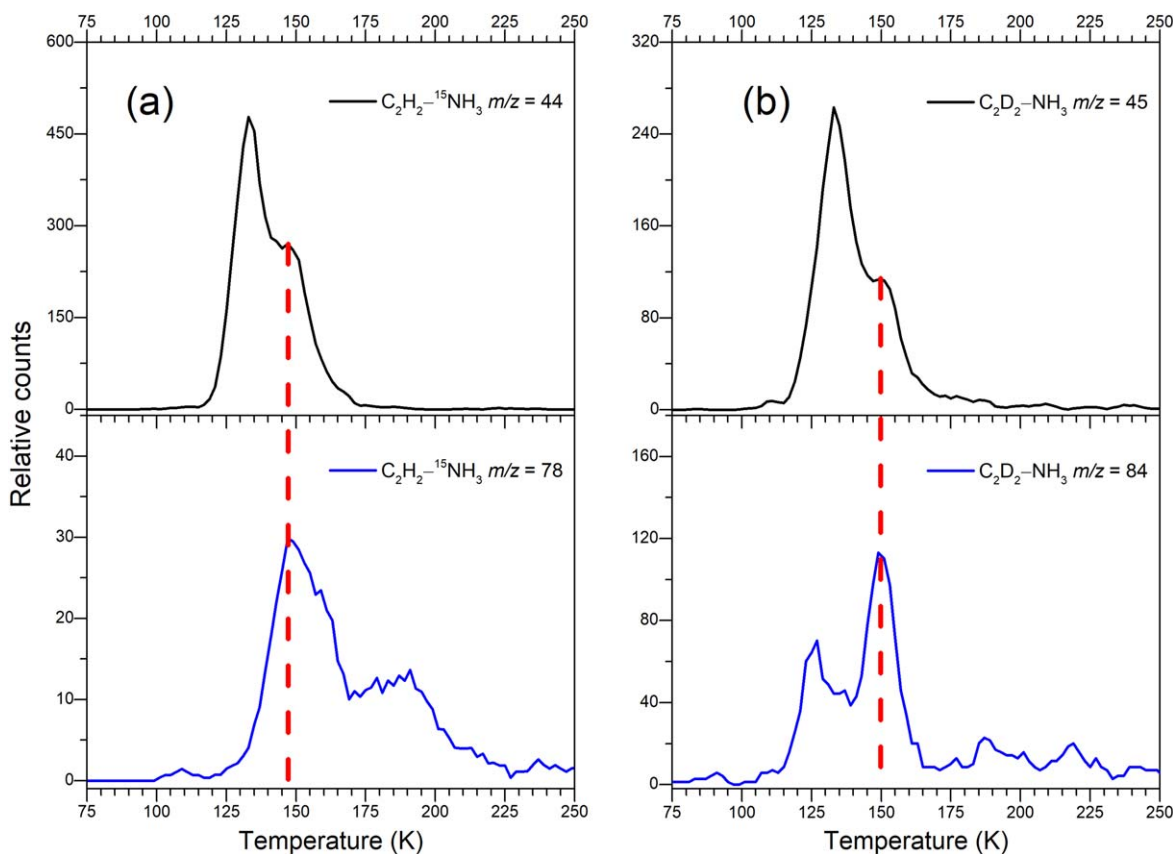
Figure 7. TPD profiles of (a) $m/z = 44$ ($C_2H_5^{15}N$) and $m/z = 78$ ($C_2H_9^{15}N_3$) from irradiated $C_2H_2–^{15}NH_3$ ices and (b) $m/z = 45$ ($C_2D_2H_3N$) and $m/z = 84$ ($C_4D_4N_2$) from irradiated $C_2D_2–NH_3$ ices. The photon energies of those experiments are 9.80 eV. The red dashed lines in panel (a) indicate the shoulder peak of $C_2H_5^{15}N$ ($m/z = 44$) that originates from the photofragments of $C_2H_9^{15}N_3$ ($m/z = 78$). The red dashed lines in panel (b) indicate the shoulder peak of $C_2D_2H_3N$ ($m/z = 45$) that originates from the photofragments of $C_4D_4N_2$ ($m/z = 84$).
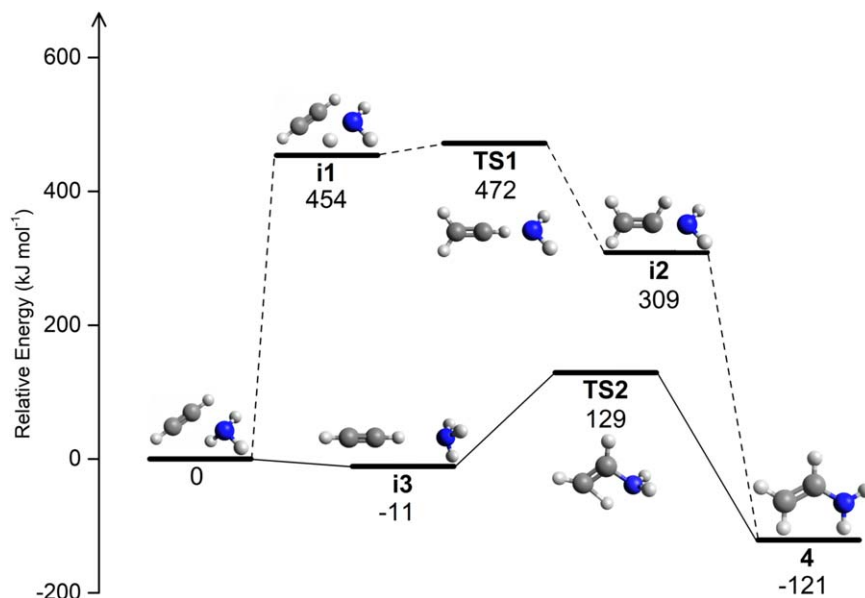
Figure 8. Gas-phase reaction scheme revealing radical–radical and molecular pathways to vinylamine.

Appendix

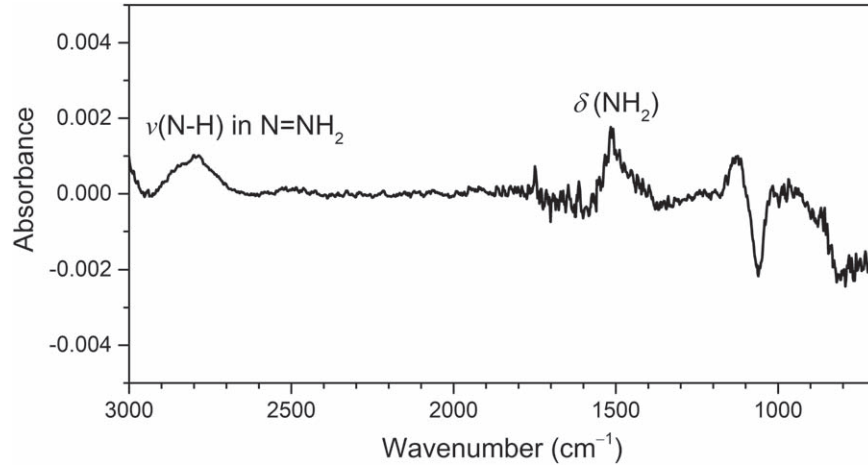The difference FTIR spectrum between the irradiated and pristine acetylene-ammonia ice mixture and the FTIR spectra for isotopically labeled ices (C_2D_2-NH_3, C_2H_2-$^{15}NH_3$) are provided here in Figure A1 and Figure A2. Error limits of IE for molecules used in this paper and computed IE of distinct C2H5N isomers are provided here in Table A1 and Table A2. FTIR absorption features for isotopically labeled ices (C_2D_2-NH_3, C_2H_2-$^{15}NH_3$) ice mixtures are provided in Table A3.

Figure A1. Difference infrared spectrum during 3000–700 cm^{-1} between the irradiated and pristine acetylene–ammonia ice mixture.
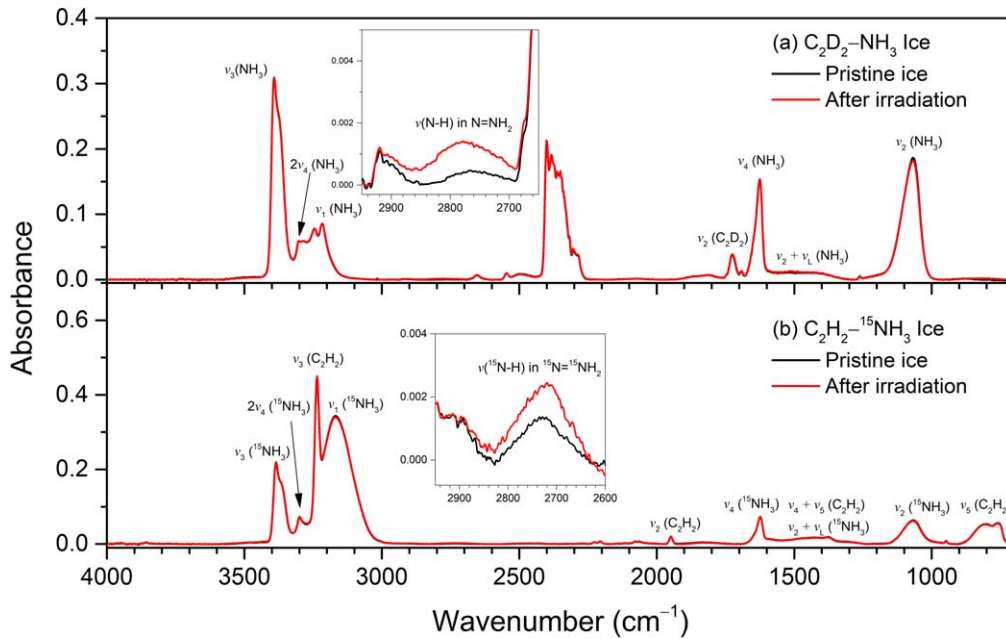
Figure A2. Infrared spectra for C_2D_2–NH_3 ice and C_2H_2–$^{15}NH_3$ ice before (black) and after (red) irradiation of 10 nA for 5 minutes with detailed assignments compiled in Table A3.

Table A1
Error Limits of Molecules Composed of Carbon, Nitrogen, and Hydrogen, Which Were Determined from the Evaluated Experimental Ionization Energies and Computed Ionization Energies at the CCSD(T)/CBS Level with CCSD(T)/aug-cc-pVTZ Zero-Point Correction

Isomers	Experimental IE (eV)	Experimental Error Limits (eV)	Computed IE (eV)	Computed IE—Experimental IE (max) (eV)	Computed IE—Experimental IE (min) (eV)
Hydrogen cyanide HCN	13.60 ± 0.01[1]	13.59–13.61	13.57	−0.04	−0.02
Acetonitrile CH_3CN	12.20 ± 0.01[2]	12.19–12.21	12.20	−0.01	+0.01
Methyl Isocyanide CH_3NC	11.24 ± 0.01[2]	11.23–11.25	11.25	+0.0	+0.02
2H-Azirine c-H_2CCHN	10.05 ± 0.03[2]	10.02–10.08	10.02	−0.06	+0.0
				Average −0.03 ± 0.03	Average +0.00 ± 0.02
				Error limits −0.06–0.00	Error limits −0.02 ± 0.02
				Combined error limits −0.06 ± 0.02	

References. (1) Lias 2018; (2) Turner et al. 2021.

Table A2
Computed Adiabatic Ionization Energies of Distinct C_2H_5N Isomers at the CCSD(T)/CBS Level with CCSD(T)/aug-cc-pVTZ ZPVE Correction, Along with Error Limits from Table A1

Isomers	Computed IE (eV)	Corrected IE after Error Analysis (eV)	Corrected IE with Electric Field Effect (eV)
Cis-ethanimine (1a)	9.54	9.48–9.56	9.45–9.53
Trans-ethanimine (1b)	9.53	9.47–9.55	9.44–9.52
Aziridine (2)	9.32	9.26–9.34	9.23–9.31
N-methylmethanimine (3)	9.14	9.08–9.16	9.05–9.13
Vinylamine (4)	8.14	8.08–8.16	8.05–8.13

Note. The offset of 0.03 eV was subtracted to correct for the electric field effect.

Table A3
Infrared Absorption Features for C_2D_2–NH_3 and C_2H_2–$^{15}NH_3$ Ice Mixtures before and after Electronic Irradiation at 10 K

C_2D_2–NH_3 Ice		C_2H_2–$^{15}NH_3$ Ice		Assignment	Reference
Absorption Peaks (cm^{-1})	New Absorption Peaks after Irradiation (cm^{-1})	Absorption Peaks (cm^{-1})	New Absorption Peaks after Irradiation (cm^{-1})		
		758		C_2H_2 (ν_5)	1
1071		1065		$NH_3/^{15}NH_3$ (ν_2)	2
1304, 1388, 1466		1299, 1373, 1435		$NH_3/^{15}NH_3$ ($\nu_2+\nu_L$)	1
1626		1623		$NH_3/^{15}NH_3$ (ν_4)	2
1724				C_2D_2 (ν_2)	1
		1948		C_2H_2 (ν_2) C_2H_2 ($2\nu_4+\nu_5$)	1
2382				C_2D_2 (ν_3)	1
		2752		C_2H_2 ($\nu_2+\nu_5$)	1
	2781		2722	N–H stretching in N=NH$_2$	3
3216		3172		$NH_3/^{15}NH_3$ (ν_1)	2
		3239		C_2H_2 (ν_3)	1
3301		3299		$NH_3/^{15}NH_3$ ($2\nu_4$)	2
3394		3385		$NH_3/^{15}NH_3$ (ν_3)	2

References. (1) Abplanalp & Kaiser 2020; (2) Zheng et al. 2008; (3) Socrates 2004.

ORCID iDs

Jia Wang https://orcid.org/0000-0002-3795-8699
Ryan C. Fortenberry https://orcid.org/0000-0003-4716-8225
Ralf I. Kaiser https://orcid.org/0000-0002-7233-7206

References

Abplanalp, M. J., Borsuk, A., Jones, B. M., & Kaiser, R. I. 2015, ApJ, 814, 45
Abplanalp, M. J., Förstel, M., & Kaiser, R. I. 2016, CPL, 644, 79
Abplanalp, M. J., Jones, B. M., & Kaiser, R. I. 2018, PCCP, 20, 5435
Abplanalp, M. J., & Kaiser, R. I. 2020, ApJ, 889, 3
Arumainayagam, C. R., Garrod, R. T., Boyer, M. C., et al. 2019, ChSRv, 48, 2293
Becke, A. D. 1988, PhRvA, 38, 3098
Becke, A. D. 1993, JChPh, 98, 5648
Belloche, A., Menten, K. M., Comito, C., et al. 2008, A&A, 482, 179
Bennett, C. J., Jamieson, C. S., Osamura, Y., & Kaiser, R. I. 2006, ApJ, 653, 792
Bergantini, A., Zhu, C., & Kaiser, R. I. 2018, ApJ, 862, 140
Bernstein, M. P., Sandford, S. A., Allamandola, L. J., Chang, S., & Scharberg, M. A. 1995, ApJ, 454, 327

Bøgelund, E. G., McGuire, B. A., Hogerheijde, M. R., van Dishoeck, E. F., & Ligterink, N. F. W. 2019, A&A, 624, A82
Boogert, A. C. A., Gerakines, P. A., & Whittet, D. C. B. 2015, ARA&A, 53, 541
Bouilloud, M., Fray, N., Bénilan, Y., et al. 2015, MNRAS, 451, 2145
Cable, M. L., Vu, T. H., Maynard-Casely, H. E., Choukroun, M., & Hodyss, R. 2018, ESC, 2, 366
Coustenis, A., Achterberg, R. K., Conrath, B. J., et al. 2007, Icar, 189, 35
Drouin, D., Couture, A. R., Joly, D., et al. 2007, Scanning, 29, 92
Förstel, M., Bergantini, A., Maksyutenko, P., Góbi, S., & Kaiser, R. I. 2017, ApJ, 845, 83
Forstel, M., Maksyutenko, P., Jones, B. M., et al. 2015, ChemPhysChem, 16, 3139
Fourikis, N., Takagi, K., & Morimoto, M. 1974, ApJ, 191, L139
Frigge, R., Zhu, C., Turner, A. M., et al. 2018, ApJ, 862, 84
Frisch, M. J., Trucks, G. W., Schlegel, H. B., et al. 2016, Gaussian 16 Rev. C. 01 (Wallingford, CT: Gaussian Inc.)
Fulchignoni, M., Ferri, F., Angrilli, F., et al. 2005, Natur, 438, 785
Hagen, W., Allamandola, L. J., & Greenberg, J. M. 1979, Ap&SS, 65, 215
Herbst, E. 2014, PCCP, 16, 3344
Hollis, J. M., Lovas, F. J., Remijan, A. J., et al. 2006, ApJ, 643, L25
Holtom, P. D., Bennett, C. J., Osamura, Y., Mason, N. J., & Kaiser, R. I. 2005, ApJ, 626, 940
Hudson, R. L., Ferrante, R. F., & Moore, M. H. 2014, Icar, 228, 276
Jefferts, K. B., Penzias, A. A., & Wilson, R. W. 1970, ApJL, 161, L87
Jones, B. M., & Kaiser, R. I. 2013, JPCL, 4, 1965
Kaiser, R. I., & Roessler, K. 1998, ApJ, 503, 959
Kaiser, R. I., Stockton, A. M., Kim, Y. S., Jensen, E. C., & Mathies, R. A. 2013, ApJ, 765, 111
Kendall, R. A., Dunning, T. H., & Harrison, R. J. 1992, JChPh, 96, 6796
Kim, Y. S., & Kaiser, R. I. 2011, ApJ, 729, 68
Kleimeier, N. F., Abplanalp, M. J., Johnson, R. N., et al. 2021a, ApJ, 911, 24
Kleimeier, N. F., Eckhardt, A. K., & Kaiser, R. I. 2021b, JACS, 143, 14009
Kleimeier, N. F., Eckhardt, A. K., Schreiner, P. R., & Kaiser, R. I. 2020, Chem, 6, 3385
Kolesniková, L., Belloche, A., Koucký, J., et al. 2022, A&A, 659, A111
Lee, C., Yang, W., & Parr, R. G. 1988, PhRvB, 37, 785
Lias, S. G. 2018, NIST Standard Reference Database, 20899
Loomis, R. A., Zaleski, D. P., Steber, A. L., et al. 2013, ApJL, 765, L9
Marks, J. H., Wang, J., Evseev, M. M., et al. 2023, ApJ, 942, 43
Marks, J. H., Wang, J., Fortenberry, R. C., & Kaiser, R. I. 2022, PNAS, 119, e2217329119
Martin, J. M. L., & Lee, T. J. 1996, CPL, 258, 136
McClure, M. K., Rocha, W. R. M., Pontoppidan, K. M., et al. 2023, NatAs, 7, 431
McKellar, A. 1940, PASP, 52, 187
Miller, J. A., & Klippenstein, S. J. 2004, PCCP, 6, 1192
Moore, M. H., & Donn, B. 1982, ApJ, 257, L47

Morton, R. J., & Kaiser, R. I. 2003, P&SS, 51, 365
Naden Robinson, V., Wang, Y., Ma, Y., & Hermann, A. 2017, PNAS, 114, 9003
Naraoka, H., Takano, Y., Dworkin, J. P., et al. 2023, Sci, 379, eabn9033
Niemann, H. B., Atreya, S. K., Demick, J. E., et al. 2010, JGR, 115, E12006
Ohishi, M., Suzuki, T., Hirota, T., Saito, M., & Kaifu, N. 2019, PASJ, 71, 86
Parker, E. T., McLain, H. L., Glavin, D. P., et al. 2023, GeCoA, 347, 42
Peterson, K. A., & Dunning, T. H. 1995, JChPh, 102, 2032
Quan, D., Herbst, E., Corby, J. F., Durr, A., & Hassel, G. 2016, ApJ, 824, 129
Raghavachari, K., Trucks, G. W., Pople, J. A., & Head-Gordon, M. 1989, CPL, 157, 479
Rivilla, V. M., Jimenez-Serra, I., Martin-Pintado, J., et al. 2021, PNAS, 118, e2101314118
Rivilla, V. M., Jimenez-Serra, I., Martin-Pintado, J., et al. 2022, FrASS, 9, 876870
Rubin, R. H., Swenson, G. W., Jr, Benson, R. C., Tigelaar, H. L., & Flygare, W. H. 1971, ApJ, 169, L39
Satorre, M. Á., Leliwa-Kopystynski, J., Santonja, C., & Luna, R. 2013, Icar, 225, 703
Sharma, M. K., Melosso, M., & Chandra, S. 2023, NewA, 98, 101928
Shimoyama, A., & Ogasawara, R. 2002, OLEB, 32, 165
Sil, M., Gorai, P., Das, A., et al. 2018, ApJ, 853, 139
Singh, S., McCord, T. B., Combe, J. P., et al. 2016, ApJ, 828, 55
Singh, S. K., Zhu, C., La Jeunesse, J., Fortenberry, R. C., & Kaiser, R. I. 2022, NatCo, 13, 375
Socrates, G. 2004, Infrared and Raman Characteristic Group Frequencies: Tables and Charts (3rd ed.; Chichester: Wiley)
Strazzulla, G., & Johnson, R. E. 1991, in Comets in the Post-Halley Era, ed. R. L. Newburn, M. Neugebauer, & J. Rahe (Dordrecht: Springer), 243
Thakur, A. C., & Remsing, R. C. 2023, ESC, 7, 479
Turner, A. M., Abplanalp, M. J., & Chen, S. Y. 2015, PCCP, 17, 27281
Turner, A. M., Chandra, S., Fortenberry, R. C., & Kaiser, R. I. 2021, ChemPhysChem, 22, 985
Turner, A. M., & Kaiser, R. I. 2020, Acc. Chem. Res., 53, 2791
Turner, B. E., Liszt, H. S., Kaifu, N., & Kisliakov, A. G. 1975, ApJ, 201, L149
VonDrasek, W. A., Okajima, S., & Hessler, J. P. 1988, ApOpt, 27, 4057
Waite, J. H., Niemann, H., Yelle, R. V., et al. 2005, Sci, 308, 982
Wang, J., Marks, J. H., Tuli, L. B., et al. 2022, JPCA, 126, 9699
Werner, H.-J., Knowles, P. J., Knizia, G., Manby, F. R., & Schütz, M. 2012, WIREs Comput. Mol. Sci., 2, 242
Werner, H.J., Knowles, P. J., Manby, F. R., et al. 2020, JChPh, 152, 144107
Yeghikyan, A. G. 2011, Ap, 54, 87
Yelle, R. V., Vuitton, V., Lavvas, P., et al. 2010, FaDi, 147, 31
Zeng, S., Jiménez-Serra, I., Rivilla, V. M., et al. 2018, MNRAS, 478, 2962
Zeng, S., Jiménez-Serra, I., Rivilla, V. M., et al. 2021, ApJL, 920, L27
Zheng, W., Jewitt, D., Osamura, Y., & Kaiser, R. I. 2008, ApJ, 674, 1242
Zhu, C., Frigge, R., Turner, A. M., et al. 2018, ChCom, 54, 5716